IEEE Access
Multidisciplinary ⋮ Rapid Review ⋮ Open Access Journal

Received 18 May 2022, accepted 9 July 2022, date of publication 19 July 2022, date of current version 22 July 2022.

Digital Object Identifier 10.1109/ACCESS.2022.3192463

RESEARCH ARTICLE

Non-Invasive Full Rheological Characterization via Combined Speckle and Brillouin Microscopy

JOHANNES WENZEL[1,2], NIKLAS RÜPRICH[1,2], KARSTEN SPERLICH[3,4], OLIVER STACHS[3,4], MELANIE SCHÜNEMANN[3,4], COLETTE LEYH[3], STEFAN KALIES[1,2], AND ALEXANDER HEISTERKAMP[1,2]

[1]Institute of Quantum Optics, Leibniz University Hannover, 30167 Hannover, Germany
[2]Lower Saxony Centre for Biomedical Engineering, Implant Research and Development (NIFE), 30625 Hannover, Germany
[3]Department of Ophthalmology, Rostock University Medical Center, 18057 Rostock, Germany
[4]Department of Life, Light and Matter, University of Rostock, 18059 Rostock, Germany

Corresponding author: Johannes Wenzel (wenzel@iqo.uni-hannover.de)

This work was supported by the Deutsche Forschungsgemeinschaft (DFG) under Project 405601114.

ABSTRACT Rheology serves to measure the deformation and flow of materials. Its associated quantities, for example, the Young's modulus, shear modulus, bulk modulus, or longitudinal modulus, are important in the biomedical field, in particular for soft materials, to characterize the response of materials to external force. Usually, mechanical probes, in particular rheometers or atomic force microscopy, are used to characterize these quantities. In the last decade, optical measurements have been derived to obtain these quantities even in small sample volumes. However, usually only one quantity is evaluated using optical techniques, such as Brillouin microscopy, which does not allow a full rheological characterization. The latter requires measuring at least two quantities, which allows for calculating all further rheological properties. In this paper, we aim to close this gap by combining two optical rheology methods, Brillouin microscopy to measure the longitudinal modulus and Laser Speckle Rheology for the shear modulus. We built an optical setup that allows the non-contact and hence non-destructive and non-invasive measurement of both quantities simultaneously in the same sample using a 780 nm, narrow linewidth (∼50 kHz) laser system. We evaluate our approach using defined samples of glycerol and polydimethylsiloxane and we demonstrate image acquisition using the combined setup. We also investigate porcine corneae, as biological samples, and demonstrate direct measurement of longitudinal modulus and shear modulus and calculation of Young's modulus, bulk modulus, and the Poission ratio, which are all in good agreement with published quantities. In the future, our approach allows for full characterization of the rheology of biological specimens.

INDEX TERMS Biomechanics, Brillouin scattering, cornea, rheology, speckle.

I. INTRODUCTION

The elasticity is an important quantity of soft materials. In the field of biomedicine, it is, for example, applied to characterize implant materials, as control of corneal stiffness, or to further characterize tissue sections [1]–[3]. In the future, it might become a further clinical parameter, for instance, in Keratoconus diagnosis where it can assist to assess the biomechanical state of the cornea [4]. Further, it can be applied in therapy, for instance, to measure the degree of cross linking and to assess the process of cross linking itself, with the ultimate aim to adapt cross linking protocols to the patient's needs.

In addition, in the case of designing hydrogel-nanoparticle combinations for drug delivery, the rheological properties of the combination are critical values for the performance. The inclusion of nanoparticles in hydrogels can increase the storage modulus under shear stress until a threshold concentration is reached. Therefore, measuring the stiffness of such materials is a great challenge for developing drug delivery devices [5].

In the material science, the viscosity of non-Newtonian fluids is investigated as a function of shear-rate. Especially

The associate editor coordinating the review of this manuscript and approving it for publication was Jingang Jiang.

the behavior of so-called shear thickening fluids is very interesting as material for ballistic protection devices [6].

Usually, rheological characterization of the elasticity of materials is performed using mechanical rheometers. These exert stress on the material to measure its deformation and calculate the moduli from the stress-strain curve. To characterize the biomechanics of specimens, conventionally atomic force microscopy, optical coherence elastography, and ultrasonic methods are applied [7]–[11]. The most important measurands in rheology are the Young's modulus E, shear modulus G, bulk modulus K, and longitudinal modulus M. Assuming isotropic tissue, only two of these quantities are necessary to calculate the others.

In the last decades, several optical methods, which allow to assess the rheological properties of materials have been developed. The idea of using optics has several advantages. Firstly, it enables a much higher spatial resolution. Secondly, the required sample volume is smaller compared to conventional rheological measurements. Thirdly, it enables non-destructive or even non-contact measurement of the sample. The optical methods, which have been applied to characterize cells and tissue-like structures include Optical Tweezers, Optical Coherence Elastography, Laser Speckle Rheology (LSR), and Brillouin Microscopy (BM) [1], [10], [12], [13].

BM was first applied in material sciences and was later transferred to biological samples by Scarcelli *et al.* [14], [15]. A Brillouin microscope measures the frequency shift of a narrow linewidth laser, which is generated by the interaction of the laser photons with acoustic phonons in the sample. If a photon interacts with an acoustic phonon, the phonon and photon may be destroyed and a new photon with higher energy originates. This is called the anti-stokes shift. Also, the photon can be destroyed so that a phonon and a photon with lower energy originates. This is called stokes-shift. The difference between stokes and anti-stokes-shift to the original laser frequency are equal and dependent on the laser frequency, the refractive index, the velocity of sound in the sample, as well as on the scattering angle. With this information, it is possible to calculate the longitudinal modulus of the sample by (1).

$$M = \rho \cdot \left(\frac{\upsilon_B \cdot \lambda}{2 \cdot n} \right)^2 \tag{1}$$

whereby ρ is the density, λ is the wavelength of the laser, υ_B the Brillouin shift and n is the refractive index of the sample [1], [16]. Today, several improvements of the initial technique exist, for instance, using different acquisition modalities (tandem Fabry-Perot-Interferometer, virtually imaged phased array (VIPA), two-stage VIPA) or by the application of stimulated Brillouin scattering [14], [17]–[19]. BM has also found wide application in biological sciences and has, for instance, recently been used to analyze spinal cord repair in zebrafish larvae [20].

Viscoelastic properties from dynamic light scattering was first measured by Thomas G. Mason and David A. Weitz[21], [22]. They combined the theory of Diffusing Wave Spectroscopy with the General-Stokes-Einstein equation to calculate the absolute value of the frequency dependent viscoelastic shear modulus, seen in (2).

$$\left| G^* (\omega) \right| = \left| G' (\omega) + i \cdot G'' (\omega) \right| \tag{2}$$

This is a complex number consisting of storage modulus $G'(\omega)$ and loss modulus $G''(\omega)$. The storage modulus indicates the stiffness and described by the ratio between strain and deformation. The loss modulus represents the viscosity of the sample. The group of Nadkarni *et al.* extended this to the Laser Speckle Rheology technique [23]. Here the viscoelastic shear modulus is calculated from laser speckle images. The sample is illuminated with a coherent light source. The backscattered light is strongly influenced by Brownian motion in the sample, which generates a time-varying interference pattern, called laser speckle [24]. A fast Camera (>100 fps) takes a series of images for a duration of ~2 s. With the second order autocorrelation function $g_2(t)$, the Mean-Square-Displacement (MSD) $<\Delta r^2(t)>$ is calculated and thereby the viscoelastic shear modulus. The applicability of LSR is found in material and biological science and can be used to evaluate the elasticity of hydrogels or coronary plaque [25], [26]. Mason and Weitz derived the theory for purely viscous fluids, it is important to note that the application on viscoelastic samples is just an approximation [21]. In this work only the storage modulus, also termed shear modulus, is determined.

Both, BM and LSR provide a single rheological quantity, similar to the other optical rheological techniques. Since two known quantities are sufficient for a full rheological characterization, we aimed to build a combined setup for BM and LSR, which allows the concurrent acquisition in the same sample using the same laser source. We used this setup to characterize defined chemical samples of glycerol and polydimethylsiloxane (PDMS). Additionally, we show its applicability to analyze porcine corneae. Both techniques can be applied for point acquisition but also in laser-scanning mode, which is additionally demonstrated.

II. METHODS

A. BRILLOUIN AND LASER SPECKLE MICROSCOPY

The setup is based on an external cavity diode laser system (DL pro 780, Toptica, Germany) with a wavelength of 780 nm and a small linewidth (~50 kHz) being used for BM and LSR (see Fig. 1). A glass plate serves to deflect about 4% of the laser power to a custom-made 100 mm long pure ^{85}Rb-vapor cell, to tune the laser to the transitions $F_g = 3 \rightarrow F_e$ of the D2 absorption line with F_g and F_e being the ground and excited states, respectively. The combination of a half-wave plate and a polarizing beam splitter (PBS1) cube allows for controlling the laser intensity on the sample. An Etalon (OP-7423-6743-2, LightMachinery Inc., Canada) is used for better suppression of amplified spontaneous emission (ASE). The laser is scanned over the sample using a galvo-system (GVS012/M, Thorlabs, US). The galvo-system

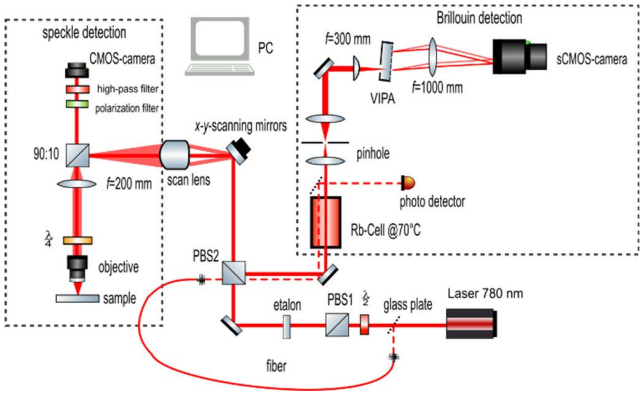

FIGURE 1. Setup combines a Brillouin microscope with a LSR microscope. The sample is illuminated by an external cavity diode laser system tuned to the transitions $F_g = 3 \rightarrow F_eD_2$ absorption line of ^{85}Rb. The backscattered light is split at a 90:10 beam splitter. 10% of the light is transmitted to the speckle detection unit, while 90% is reflected back to the scanning mirrors to get descanned and guided into the Brillouin spectrometer via a polarizing beam splitter cube. The spectrometer is based on a ^{85}RB-vapor cell, a VIPA, and an sCMOS-camera.

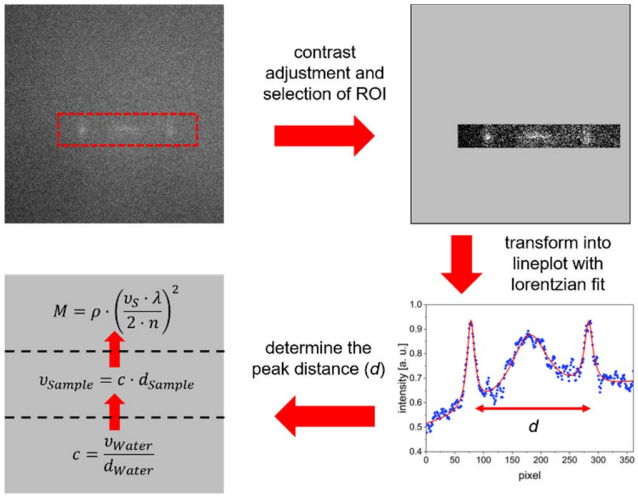

FIGURE 2. Longitudinal modulus is determined in four steps. 1. An image of the Brillouin spectrum with 1 s to 2 s integration time is captured. 2. The contrast is adjusted and a region of interest is selected. 3. The spectrum is transferred in a line-plot and the peak distance is calculated from a Lorentz fit. 4.The calibration factor of water is used to convert the distance in pixel to the Brillouin shift in GHz and this allows for determining the longitudinal modulus.

is controlled with a DAQ (USB-6003, National Instruments, US) and a customized Labview (National Instruments, US) code. The quarter-wave plate in front of the objective lens serves to change the linearly polarized laser light to circular polarization on its way to the sample and finally to linearly polarized light again with perpendicular orientation on its way to the detection units. The objective lens (10X M Plan Apo, Edmund Optics Inc., US) with a numerical aperture of 0.28 focuses the light on the sample and collects the backscattered light. A 90:10 beam splitter directs 10% of the signal to the speckle detection unit and remaining 90% to the Brillouin detection unit.

The speckle detection unit encompasses a high-pass filter to block ambient light, a polarization filter to collect the cross-polarized backscattered light only, and a camera (UI-3360, IDS Imaging Development Systems GmbH, Germany). A typical acquisition of a single point for LSR involves the capture of 2000 frames with a framerate of 325 fps and a size of 480 px × 480 px.

In the Brillouin detection unit, PBS2 separates the backscattered light, which underwent a polarization change of 90° by passing the quarter-wave plate two times, from the incoming light. The spectrometer consists of a ^{85}Rb-vapor cell, which is heated up to 70 °C to suppress the Rayleigh signal. After the cell, there is a telescope pinhole construction, with a four times magnification of the beam waist. With a 300 mm cylinder lens, the beam is focused into the VIPA and a 1000 mm lens transforms the VIPA output into spectrally and spatially resolved signals onto the camera (Andor Zyla 4.2 Plus, Oxford Instruments plc, UK). Typically, a Brillouin spectrum with 1 s to 2 s exposure time is collected at every point.

The two detection units allow for measuring Brillouin signal and laser speckle without changing the setup or moving of the sample.

B. COMPUTATIONAL ANALYSIS OF THE BRILLOUIN IMAGES

The images acquired in the Brillouin detection unit are processed using self-written Matlab (MathWorks, Inc., US) code extracting the Brillouin shift. In a preprocessing step, the contrast of the images is adjusted and a region of interest is cropped. The signal is transformed in a line plot and the peaks are fitted with a Lorentzian-curve. The distance between the Stokes and Anti-Stokes peak, which represents the Brillouin shift, is derived from the fit. At the beginning of every imaging session and between the acquisitions of two samples, the Brillouin shift of water is determined. This serves to validate the alignment of the setup, to avoid temporal fluctuations, and to calibrate the Brillouin measurements. The Brillouin shift υ_B of every unknown sample is converted from pixel to GHz with the calibration factor from water. Finally, the longitudinal modulus M of the sample is calculated by (1). All steps are outlined in Fig. 2.

C. COMPUTATIONAL ANALYSIS OF THE SPECKLE IMAGES

The Speckle images are evaluated with a self-written Python-Code based on the description of Nadkarni et al[3]. Briefly, from one image stack of 2000 speckle frames, the time depending second order autocorrelation function is calculated (see Fig. 3). The autocorrelation function is first averaged over all pixels and then over the start points t_0. Because of this, the number of frames must be greater than the length of the curve in frames added to the number of the start points. The equation is transformed into the time-dependent MSD of the Diffusing Wave Spectroscopy theory and approached with a logistic fit. To do this, we use the standardized autocorrelation curve $(g_2(t))/(g_2(0))$ with the wavenumber k of the laser

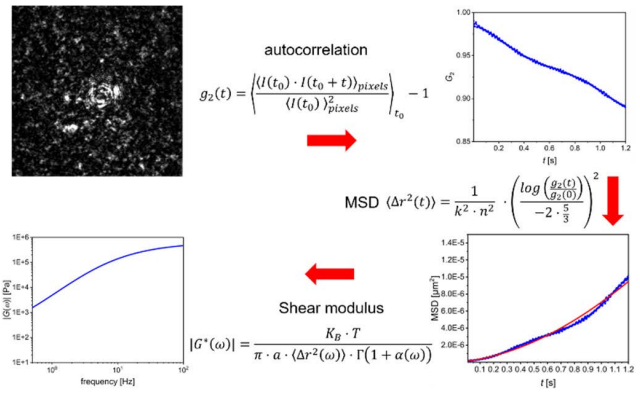

FIGURE 3. Evaluation of the Speckle images consists of four steps. 1. A speckle frame is imaged. 2. The autocorrelation function $g_2(t)$ over 2 s is determined and averaged over 1000 starting points. 3. The mean-square displacement is calculated and fitted with a logistic fit. 4. The complex shear modulus and its real and imaginary part are determined.

and the refractive index n of the sample. The fit is inserted in the General-Stokes-Einstein equation and the time dependency is changed to a frequency dependency. To calculate the absolute value of the viscoelastic shear modulus (3), the log-log-slope (4) of the MSD and the gamma-function have to be computed.

$$\left|G^*(\omega)\right| = \frac{K_B\cdot T}{\left(\pi\cdot a\cdot\langle\Delta r^2(\omega)\rangle\cdot\Gamma\left(1+\alpha(\omega)\right)\right)} \tag{3}$$

$$\alpha(\omega) = t\cdot\left(\frac{d\log\left(\langle\Delta r^2(t)\rangle\right)}{dt}\right)|_{(\omega=1/t)} \tag{4}$$

Therefore, the particle size a, the Boltzmann constant K_B and the room temperature T need to be known. Further the storage modulus $G'(\omega)$ with the restriction $0 < \alpha(\omega) < 1$ can be derived, by (5)[3].

$$G'(\omega) = \left|G^*(\omega)\right|\cdot cos\left(\frac{\pi}{2}\cdot\alpha(\omega)\right) \tag{5}$$

For values of $\alpha(\omega) > 1$, the measurements are in a super-diffuse region, where not only Brownian motion induces particle drifts. Possible causes are the sample itself or environmental vibrations [3], [27], [28]. In our measurements the values at lower frequencies < 10 Hz are affected from this. Because of this and because the shear modulus is conventionally measured at low frequencies our further analysis is based on the values at 10 Hz [29].

D. PREPARATION AND CHARACTERIZATION OF REFERENCE SAMPLES

PDMS is frequently used as tissue phantom and its optical and mechanical properties are well known. Its shear modulus varies in a range of 100 kPa to 3 MPa [30]. The longitudinal modulus depends directly on the longitudinal sound velocity, which ranges from 1050 m/s to 1219 m/s according to the molecular weight and the cross-link density. This results in an expected longitudinal modulus of 1.14 GPa to 1.54 GPa [31], [32].

Glycerol-water mixtures are well characterized by Nadkarni *et al.* and have previously been used to evaluate the LSR [33]. For a 90%:10% glycerol-water mixture, the shear modulus at 10 Hz varies between 10 Pa to 100 Pa [33].

The expected Brillouin shift for water and glycerol are 5.12 GHz and 7.24 GHz, respectively [34]. To estimate a literature value of our mixture, we calculate the longitudinal modulus of water M_w and glycerol M_g from their Brillouin shift. Provided, that the expected longitudinal modulus of the mixture M_m can be calculated by (6), with the volume fraction of water $\epsilon \approx 0.75$ and the longitudinal moduli $M_g = 4.65$ GPa and $M_w = 2.25$ GPa of glycerol and water to $M_m = 2.58$ GPa [35], [36].

$$\frac{1}{M_m} \approx \frac{1-\epsilon}{M_g} + \frac{\epsilon}{M_w} \tag{6}$$

In both samples, TiO_2 particles (anatase) (Merck KGaA, Germany) with a size of around 200 nm were added to increase scattering for speckle acquisition.

To create the PDMS sample, a 1:10 ratio of curing agent and silicon (DOW Europe GmbH, Germany) doped with 0.25% w/w TiO2 is mixed and the sample is cured for three hours at 60° C. To create a glycerol sample, a water glycerol mixture with 25% v/v glycerol is doped with 0.068% w/v TiO2. In total, 16 independent PDMS and glycerol samples were measured. In each sample, the longitudinal modulus and the shear modulus were evaluated at five different points. The median value of these five measurements was used to determine the longitudinal and shear modulus of a single sample, subsequently the moduli of all samples were averaged and the mean value was used for further statistics. For the calculations, for 25%-glycerol, a density of 1071 kg/m^3 and a refractive index of 1.36 were used based on the literature [37], [38]. PDMS has a density of 1035 kg/m^3 calculated from the volume and weight measurements and a refractive index of 1.39 [39]. The results of all samples and both moduli were visualized using the software OriginPro 2020 (OriginLab, US). The box plots are characterized by the upper line of the box, 75th percentile; lower line of the box, 25th percentile; horizontal bar within the box, median; upper bar outside the box, 90th percentile; lower bar outside the box, 10th percentile. Dots represent outliers. Statistical analysis was performed using a Student's t-test.

For image acquisition, a new PDMS sample was prepared, as explained above. A randomly selected hole is cut off in the sample and filled with a 12.5%-glycerol mixture, doped with 0.068% w/v TiO2 particles. At the transition of the materials, a scan area of around 200 μm $\times$ 200 μm in 20 μm steps was defined and both detection methods were applied. In the case of the speckle scan, at every point, 400 frames with a frame rate of 200 fps were captured. The autocorrelation function was averaged over 60 pixels $\times$ 60 pixels. For the longitudinal modulus measurement, a Brillouin spectrum was acquired for 1.5 s and evaluated at every point.

E. PREPARATION AND CHARACTERIZATION OF PORCINE CORNEA

Porcine eyes were obtained from a slaughterhouse near Rostock (Germany) and examined at an average of 2 days post mortem. Before imaging, the eyes were kept in a humidified, chilled environment. A corneal disk of 8 mm was dissected from the rest of the eye using an 8 mm biopsy punch and stored into a 0.9% NaCl-solution during the measurement. Both, the anterior and posterior surface of the cornea were measured in a central and peripheral region. Each region of every eye was measured five times for both moduli.

The median value of these five measurements was determined and used to calculate the average longitudinal and shear modulus of all samples in a single region using a density of 1062 kg/m^3 [40] and a refractive index of 1.375[41]. Both moduli were graphically represented using the software OriginPro. Box plots of all eyes are characterized by the upper line of the box, 75th percentile; lower line of the box, 25th percentile; horizontal bar within the box, median; upper bar outside the box, 90th percentile; lower bar outside the box, 10th percentile. Dots represent outliers. Statistical analysis was performed using a Student's *t*-test.

III. RESULTS AND DISCUSSION

A. THE APPLICATION OF COMBINED SPECKLE AND BM ENABLES A FULL RHEOLOGICAL CHARACTERIZATION OF SAMPLES

In the first set of experiments, we aimed to verify the applicability of combined speckle and Brillouin microscopy in defined chemical samples and analyzed 25%-glycerol and PDMS (see Fig. 4). For 25%-glycerol, we obtained a longitudinal modulus of about 3.06 GPa and a shear modulus of about 0.159 kPa. In the case of PDMS, the longitudinal Modulus is 1.50 GPa, while the shear modulus results in 555 kPa. In particular, both moduli are significantly different between the samples (*t*-test, p<0.0001). The obtained values are in good agreement with our literature research, G_{PDMS}: 100 kPa to 3 MPa, M_{PDMS}: 1.14 GPa to 1.54 GPa, G_{glycerol}: 10 Pa to 100 Pa, M_{glycerol}: 2.58 GPa [30]–[34]. The minor deviations are explained in the following. The theoretical M value of the 25%-glycerol is lower than the results of our experiment, which might be associated with unavoidable evaporation during sample measurement. The results of the shear modulus for our glycerol sample are higher than the values from Nadkarni *et al.* (10 to 100 Pa) which could be due to different raw materials or attributed to the lower frame rate of the CMOS camera in our measurements [33]. In addition, the concentration of the scattering particles could be lower, because a lower scattering coefficient might lead to a slower falling autocorrelation curve [33]. However, higher concentrations were not feasible, as the Brillouin signal would be too weak to measure with our setup. The measurements allowed us to calculate further rheological moduli, summarized in Table 3.1.

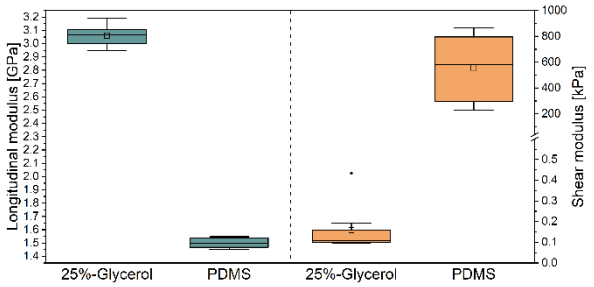

FIGURE 4. Box plot of single point measurements of PDSM and 25%-glycerol. For each sample the median of 5 measurements were taken and in total 8 independent samples of every material were analyzed. The longitudinal modulus of 25%-glycerol is about 3.06 GPa and the shear modulus is approximately 0.159 kPa. In the case of PDMS, the longitudinal Modulus is 1.50 GPa, while the shear modulus results in 555 kPa.

TABLE 1. Results of 25%-glycerol and PDMS and calculated additional moduli and corresponding equations.

Modulus	Equation[42]	25%-glycerol	PDMS
	Experimental Data		
Shear modulus [kPa]	G	0.159	555
Brillouin shift [GHz]	υ_{B}	5.89	4.29
	Calculated Data		
Longitudinal modulus [GPa]	$M = \rho \cdot \left(\frac{\upsilon_{\mathrm{B}} \cdot \lambda}{2 \cdot n}\right)^2$	3.06	1.50
Difference from Poisson ratio	$\Delta\nu = 0.5 - \nu = 0.5 - \frac{M - 2 \cdot G}{2 \cdot M - 2 \cdot G}$	$2.59 \cdot 10^{-8}$	$1.84 \cdot 10^{-4}$
Bulk modulus [GPa]	$K = M - \frac{4 \cdot G}{3}$	3.06	1.5
Young`s modulus [kPa]	$E = \frac{G \cdot (3 \cdot M - 4 \cdot G)}{M - G}$	0.476	1664.8

The results show, that a higher longitudinal or bulk modulus does not necessarily imply a higher shear or Young's modulus. For investigating materials, especially of different physical states, a full rheological characterization is necessary for comparison. If M is magnitudes larger than G, it is further possible to assume with high validity K≈M and $E = (G \cdot (3 \cdot M - 4 \cdot G))/(M - G) \approx (G \cdot 3\,M)/M = 3G$.

Additionally, we evaluated whether we can obtain a microscopy image with a full rheological analysis of a sample of PDMS and 12.5%-glycerol (see Fig. 5). The longitudinal modulus of PDMS was between 1.41 GPa and 1.72 GPa and the values of the 12.5%-glycerol varied between 2.34 GPa and 2.65 GPa. The PDMS values are in good agreement with our single point measurements and the values of the 12.5 %-glycerol are, as expected, lower than the values of 25%-glycerol in the single measurements.

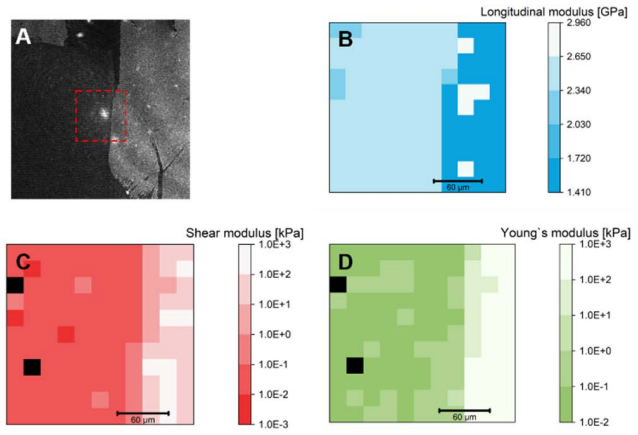

FIGURE 5. **Full rheological microscopy image of PDMS and 12.5%-glycerol. A) A confocal image of the sample, the darker part on the left side of the image is the 12.5%-glycerol and the right part is the PDMS. Both materials are good to distinguish because of the different TiO_2 concentrations. The red dashed square marks the scanning area and the bright point in the middle is the central back reflection of the laser. B and C) A two-dimensional measurement of the longitudinal and shear modulus. In both scans the transition from PDMS to 12.5%-glycerol is well recognizable. D) The green map represents the calculated Young's modulus. Each pixel is determined by the corresponding pixels from the longitudinal and shear modulus map.**

With both methods, a two-dimensional measurement is possible and enables the calculation of two-dimensional images of the other moduli. This is shown in Fig. 5D with the Young's modulus, representatively for all other moduli.

B. THE APPLICATION OF COMBINED SPECKLE AND BM ALLOWS A MORE PRECISE CHARACTERIZATION OF CORNEAL STIFFNESS

A clinical relevant setting of rheological characterization is the determination of corneal stiffness, for instance, to evaluate keratoconus. Therefore, as a proof-of-example, we examined porcine corneas and determined both longitudinal and shear modulus on both sides of the cornea in the central and peripheral regions, respectively (see Fig. 6 and 7). Because corneae are not isotropic and we measure the moduli just in one direction, the determined values are not generally valid. This have to be known when the results are compared with other measurements, but for this work it is not further relevant.

For the anterior side of the cornea, we obtained a longitudinal modulus of 2.63 GPa in the central region, and a statistically insignificant different value of 2.62 GPa in the peripheral region ($p=0.61$, t-test). For the posterior side of the cornea, we obtained a longitudinal modulus of 2.43 GPa in the central region, and a statistically insignificant different value of 2.45 GPa in the peripheral region ($p=0.30$, t-test). However, the central and peripheral anterior regions were statistically significantly different ($p<0.001$, t-test) from their posterior counterparts. Scarcelli *et al.* obtained corresponding measurements on the posterior and anterior sides of the cornea, which might indicate that the anterior part seems to be stiffer than the posterior part[8] However, another reason

TABLE 2. **Results of the cornea and calculated additional moduli and corresponding equations.**

Sample	A-C	A-P	P-C	P-P
Experimental Data				
Shear modulus [kPa]	173.3	147.1	715.2	275.1
Brillouin shift [GHz]	5.53	5.51	5.31	5.33
Calculated Data				
longitudinal modulus [GPa]	2.63	2.62	2.43	2.45
Difference from Poisson ratio	$3.61\cdot10^{-7}$	$1.93\cdot10^{-7}$	$2\cdot10^{-6}$	$1.67\cdot10^{-6}$
Bulk modulus [GPa]	2.63	2.62	2.43	2.45
Young`s modulus [kPa]	519.7	441.2	2145.4	825.2

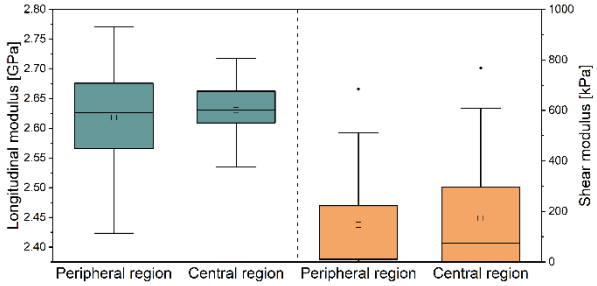

FIGURE 6. **Longitudinal and shear modulus of the anterior regions of the cornea. For each region the median of five measurements were taken and in total 18 eyes were evaluated. The longitudinal moduli of the peripheral and central region are about 2.62 GPa and 2.63 GPa. The shear moduli are approximately 147.1 kPa (peripheral) and 173.3 kPa (central).**

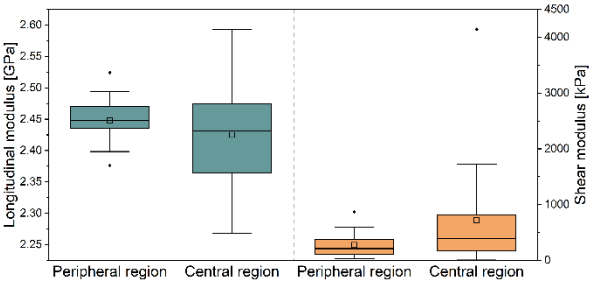

FIGURE 7. **Analysis of the posterior regions of the cornea. For each region the median of five measurements were taken and in total 18 eyes were evaluated. The longitudinal moduli of the peripheral and central regions are about 2.45 GPa and 2.43 GPa. The shear moduli are approximately 275.1 kPa (peripheral) and 715.2 kPa (central).**

for the lower longitudinal modulus in the posterior part could also be a higher degree of hydration [35], [41]. Other studies detected a higher hydration of the posterior part of the cornea for bovine and rabbits[43], [44]. This might affect the Brillouin signal.

The shear modulus of the anterior central region was 173.3 kPa, while the shear modulus in the peripheral region was statistically insignificantly different with 147.1 kPa

(p=0.77, *t*-test). The posterior central region yielded a shear modulus of 715.2 kPa and a statistically insignificantly different peripheral shear modulus of 275.1 kPa (p=0.078, *t*-test). Again, the central and peripheral anterior regions were statistically insignificantly different (p<0.13, *t*-test) from their posterior counterparts. This indicates that the posterior part of the cornea is stiffer. The corneal posterior side contains the Descemet's membrane and the endothelium. This is in agreement with measurements on human and rabbit cornea, which also show a higher stiffness in these regions [45], [46].

IV. SUMMARY AND CONCLUSION

We demonstrate combined LSR and BM to determine a full rheological profile of biological samples. To the best of our knowledge this is the first non-invasive full characterization of all rheological moduli of single samples.

With both methods, the differences between various materials and further between regional variations of biological tissues were determined. The relative changes in the shear moduli are greater than the relative changes in the longitudinal moduli, so the shear modulus is more sensitive to small differences. However, we also observed greater uncertainties, which demands a consequent statistical validation.

Further, we demonstrated the possibility for a full two-dimensional rheological characterization with our setup. This enabled us to detect rheological differences with a spatial resolution of around 20 μm. However, this scanning approach currently requires long integration times limiting its applicability for many biological applications, especially if other factors such as sample hydration or sample movement influence the measurement.

A drawback of speckle imaging is the necessity for scattering samples. A high scattering provides sufficient backscattered light such that high frame rates are possible or less laser power is needed. However, this also limits the applicability of the same sample for Brillouin microscopy, as in strongly scattering samples the Brillouin peak is weak. Therefore, currently, our approach cannot be generalized to all biological samples.

A drawback of BM is the uncertainty, which is associated with the degree of hydration of the investigated sample. Our corneal measurements obtained by BM indicated that the anterior side seems to have a higher a higher longitudinal modulus than the posterior side. This is in contrast to our speckle analysis and studies on human and rabbit corneae [45], [46]. It might be attributed to the higher hydration of the posterior side. One limitation we did not mentioned in this analysis, is that we measure the shear modulus at a low frequency (10 Hz) and the longitudinal modulus in the GHz range [1], [29]. At the current state of the art, it is not possible to measure the shear modulus in the GHz range, because exposure times of less than one nanosecond would be needed [24]. On the other side, to the best of our knowledge, there is no way to measure the longitudinal modulus in a low frequency range or concluding these values from an optical Brillouin measurement. This needs to be addressed in future studies.

REFERENCES

[1] R. Prevedel, A. Diz-Muñoz, G. Ruocco, and G. Antonacci, "Brillouin microscopy: An emerging tool for mechanobiology," Tech. Rep., 2019. [Online]. Available: https://www.nature.com/articles/s41592-019-0543-3, doi: 10.1038/s41592-019-0543-3.

[2] S. Kling and F. Hafezi, "Corneal biomechanics—A review," *Ophthalmic Physiolog. Opt.*, vol. 37, no. 3, pp. 240–252, May 2017, doi: 10.1111/opo.12345.

[3] Z. Hajjarian and S. K. Nadkarni, "Technological perspectives on laser speckle micro-rheology for cancer mechanobiology research," *J. Biomed. Opt.*, vol. 26, no. 9, Sep. 2021, Art. no. 090601, doi: 10.1117/1.JBO.26.9.090601.

[4] P. Shao, A. M. Eltony, T. G. Seiler, B. Tavakol, R. Pineda, T. Koller, T. Seiler, and S.-H. Yun, "Spatially-resolved Brillouin spectroscopy reveals biomechanical abnormalities in mild to advanced keratoconus *in vivo*," *Sci. Rep.*, vol. 9, no. 1, pp. 1–12, Dec. 2019, doi: 10.1038/s41598-019-43811-5.

[5] C. Giordano, D. Albani, A. Gloria, M. Tunesi, S. Rodilossi, T. Russo, G. Forloni, L. Ambrosio, and A. Cigada, "Nanocomposites for neurodegenerative diseases: Hydrogel-nanoparticle combinations for a challenging drug delivery," *Int. J. Artif. Organs*, vol. 34, no. 12, pp. 1115–1127, Dec. 2011, doi: 10.5301/ijao.2011.8915.

[6] F. J. Galindo-Rosales, F. J. Rubio-Hernández, and A. Sevilla, "An apparent viscosity function for shear thickening fluids," *J. Non-Newtonian Fluid Mech.*, vol. 166, nos. 5–6, pp. 321–325, Mar. 2011, doi: 10.1016/j.jnnfm.2011.01.001.

[7] P. Parot, Y. F. Dufrêne, P. Hinterdorfer, C. L. Grimellec, D. Navajas, J.-L. Pellequer, and S. Scheuring, "Past, present and future of atomic force microscopy in life sciences and medicine," *J. Mol. Recognit.*, vol. 20, no. 6, pp. 418–431, Nov. 2007, doi: 10.1002/JMR.857.

[8] G. Scarcelli, S. Kling, E. Quijano, R. Pineda, S. Marcos, and S. H. Yun, "Brillouin microscopy of collagen crosslinking: Noncontact depth-dependent analysis of corneal elastic modulus," *Investigative Ophthalmol. Vis. Sci.*, vol. 54, no. 2, pp. 1418–1425, Feb. 2013, doi: 10.1167/iovs.12-11387.

[9] F. E. Hauser, "Techniques for measuring stress-strain relations at high strain rates," *Experim. Mech.*, vol. 6, no. 8, pp. 395–402, Aug. 1966, doi: 10.1007/BF02326284.

[10] S. Wang and K. V. Larin, "Optical coherence elastography for tissue characterization: A review," *J. Biophoton.*, vol. 8, no. 4, pp. 279–302, Apr. 2015, doi: 10.1002/JBIO.201400108.

[11] X. He, E. Spoerl, J. Tang, and J. Liu, "Measurement of corneal changes after collagen crosslinking using a noninvasive ultrasound system," *J. Cataract Refractive Surg.*, vol. 36, no. 7, pp. 1207–1212, Jul. 2010, doi: 10.1016/J.JCRS.2009.12.047.

[12] H. Zhang and K.-K. Liu, "Optical tweezers for single cells," *J. Roy. Soc. Interface*, vol. 5, no. 24, pp. 671–690, Jul. 2008, doi: 10.1098/RSIF.2008.0052.

[13] Z. Hajjarian and S. K. Nadkarni, "Tutorial on laser speckle rheology: Technology, applications, and opportunities," *J. Biomed. Opt.*, vol. 25, no. 5, May 2020, Art. no. 50801, doi: 10.1117/1.JBO.25.5.050801.

[14] G. Scarcelli and S. H. Yun, "Confocal Brillouin microscopy for three-dimensional mechanical imaging," *Nature Photon.*, vol. 2, no. 1, pp. 39–43, Jan. 2008, doi: 10.1038/nphoton.2007.250.

[15] Y. Takagi and K. Kurihara, "Application of a microscope to Brillouin scattering spectroscopy," *Rev. Sci. Instrum.*, vol. 63, no. 12, pp. 5552–5555, Dec. 1992, doi: 10.1063/1.1143380.

[16] R. J. J. Rioboó, N. Gontán, D. Sanderson, M. Desco, and M. V. Gómez-Gaviro, "Brillouin spectroscopy: From biomedical research to new generation pathology diagnosis," *Int. J. Mol. Sci.*, vol. 22, no. 15, p. 8055, Jul. 2021, doi: 10.3390/ijms22158055.

[17] D. C. Liptak, J. C. Reber, J. F. Maguire, and M. S. Amer, "On the development of a confocal Rayleigh–Brillouin microscope," *Rev. Sci. Instrum.*, vol. 78, no. 1, Jan. 2007, Art. no. 016106, doi: 10.1063/1.2431181.

[18] G. Scarcelli and S. H. Yun, "Multistage VIPA etalons for high-extinction parallel Brillouin spectroscopy," *Opt. Exp.*, vol. 19, no. 11, pp. 10913–10922, May 2011, doi: 10.1364/OE.19.010913.

[19] C. W. Ballmann, J. V. Thompson, A. J. Traverso, Z. Meng, M. O. Scully, and V. V. Yakovlev, "Stimulated Brillouin scattering microscopic imaging," *Sci. Rep.*, vol. 5, no. 1, p. 18139, Nov. 2016, doi: 10.1038/srep18139.

[20] R. Schlüßler, S. Möllmert, S. Abuhattum, G. Cojoc, P. Müller, K. Kim, C. Möckel, C. Zimmermann, J. Czarske, and J. Guck, "Mechanical mapping of spinal cord growth and repair in living zebrafish larvae by Brillouin imaging," *Biophys. J.*, vol. 115, no. 5, pp. 911–923, Sep. 2018, doi: 10.1016/j.bpj.2018.07.027.

[21] T. G. Mason and D. A. Weitz, "Optical measurements of frequency-dependent linear viscoelastic Moduli of complex fluids," *Phys. Rev. Lett.*, vol. 74, no. 7, pp. 1250–1253, Feb. 1995, doi: 10.1103/PhysRevLett.74.1250.

[22] T. G. Mason, "Original contribution estimating the viscoelastic moduli of complex fluids using the generalized Stokes-Einstein equation," *Rheolog. Acta*, vol. 39, no. 4, pp. 371–378, Aug. 2000.

[23] Z. Hajjarian and S. K. Nadkarni, "Measurement of bulk mechanical properties of tissue using laser speckle rheology," in *Proc. Annu. Int. Conf. IEEE Eng. Med. Biol. Soc.*, Aug. 2011, pp. 5746–5748, doi: 10.1109/IEMBS.2011.6091422.

[24] Z. Hajjarian and S. K. Nadkarni, "Evaluating the viscoelastic properties of tissue from laser speckle fluctuations," *Sci. Rep.*, vol. 2, no. 1, pp. 1–8, Dec. 2012, doi: 10.1038/srep00316.

[25] Z. Hajjarian, H. T. Nia, S. Ahn, A. J. Grodzinsky, R. K. Jain, and S. K. Nadkarni, "Laser speckle rheology for evaluating the viscoelastic properties of hydrogel scaffolds," *Sci. Rep.*, vol. 6, no. 1, pp. 1–12, Dec. 2016, doi: 10.1038/srep37949.

[26] S. K. Nadkarni, "Laser speckle rheology and micromechanics," in *Proc. Opt. Life Sci. Congr.*, 2017, Art. no. OmM4D, doi: 10.1364/OMP.2017.OmM4D.1.

[27] T. Savin and P. S. Doyle, "Static and dynamic errors in particle tracking microrheology," *Biophys. J.*, vol. 88, no. 1, pp. 623–638, Jan. 2005, doi: 10.1529/biophysj.104.042457.

[28] T. Savin and P. S. Doyle, "Role of a finite exposure time on measuring an elastic modulus using microrheology," *Phys. Rev. E, Stat. Phys. Plasmas Fluids Relat. Interdiscip. Top.*, vol. 71, no. 4, Apr. 2005, Art. no. 041106, doi: 10.1103/PhysRevE.71.041106.

[29] G. Scarcelli, P. Kim, and S. H. Yun, "In vivo measurement of age-related stiffening in the crystalline lens by Brillouin optical microscopy," *Biophys. J.*, vol. 101, no. 6, pp. 1539–1545, Sep. 2011, doi: 10.1016/j.bpj.2011.08.008.

[30] J. C. Lotters, W. Olthuis, P. H. Veltink, and P. Bergveld, "The mechanical properties of the rubber elastic polymer polydimethylsiloxane for sensor applications," *J. Micromech. Microeng.*, vol. 7, no. 3, pp. 145–147, 1997, doi: 10.1088/0960-1317/7/3/017.

[31] M. Sinha, J. E. Mark, H. E. Jackson, and D. Walton, "A Brillouin scattering study of end-linked poly(dimethylsiloxane) networks," *J. Chem. Phys.*, vol. 117, no. 6, p. 2968, Aug. 2002, doi: 10.1063/1.1493188.

[32] S. Shin, J.-H. Ko, J. Park, Y. H. Ko, and K. J. Kim, "Pressure dependence of acoustic anomalies of polydimethylsiloxane studied by Brillouin spectroscopy," *Phys. B, Condens. Matter*, vols. 466–467, pp. 50–53, Jun. 2015, doi: 10.1016/j.physb.2015.03.025.

[33] Z. Hajjarian and S. K. Nadkarni, "Evaluation and correction for optical scattering variations in laser speckle rheology of biological fluids," *PLoS ONE*, vol. 8, no. 5, May 2013, Art. no. e65014, doi: 10.1371/journal.pone.0065014.

[34] *Brillouin Scattering Database*. Accessed: Mar. 18, 2022. [Online]. Available: http://koski.ucdavis.edu/BRILLOUIN/index.html

[35] P.-J. Wu, I. V. Kabakova, J. W. Ruberti, J. M. Sherwood, I. E. Dunlop, C. Paterson, P. Török, and D. R. Overby, "Water content, not stiffness, dominates Brillouin spectroscopy measurements in hydrated materials," *Nature Methods*, vol. 15, no. 8, pp. 561–562, Jul. 2018, doi: 10.1038/s41592-018-0076-1.

[36] D. L. Johnson, "Elastodynamics of gels," *J. Chem. Phys.*, vol. 77, no. 3, pp. 1531–1539, Aug. 1982, doi: 10.1063/1.443934.

[37] *Calculate Density and Viscosity of Glycerol/Water Mixtures*. Accessed: Mar. 22, 2022. [Online]. Available: http://www.met.reading.ac.uk/~sws04cdw/viscosity_calc.html

[38] I. P. Rosas, J. L. Contreras, J. Salmones, C. Tapia, B. Zeifert, J. Navarrete, T. Vázquez, and D. C. García, "Catalytic dehydration of glycerol to acrolein over a catalyst of Pd/LaY zeolite and comparison with the chemical equilibrium," *Catalysts*, vol. 7, no. 3, p. 73, 2017, doi: 10.3390/catal7030073.

[39] X. Zhang, J. Qiu, J. Zhao, X. Li, and L. Liu, "Complex refractive indices measurements of polymers in infrared bands," *J. Quant. Spectrosc. Radiat. Transf.*, vol. 252, Sep. 2020, Art. no. 107063, doi: 10.1016/J.JQSRT.2020.107063.

[40] J. Kampmeier, B. Radt, R. Birngruber, and R. Brinkmann, "Thermal and biomechanical parameters of porcine cornea," *Cornea*, vol. 19, no. 3, pp. 355–363, May 2000. [Online]. Available: http://journals.lww.com/corneajrnl

[41] P. Shao, T. G. Seiler, A. M. Eltony, A. Ramier, S. J. Kwok, G. Scarcelli, R. Pineda, and S. H. Yun, "Effects of corneal hydration on Brillouin microscopy *in vivo*," *Investigative Ophthalmol. Vis. Sci.*, vol. 59, no. 7, pp. 3020–3027, Jun. 2018, doi: 10.1167/iovs.18-24228.

[42] G. Mavko, T. Mukerji, and J. Dvorkin, *The Rock Physics Handbook*. Cambridge, U.K.: Cambridge Univ. Press, 2009, doi: 10.1017/CBO9780511626753.

[43] J. A. Castoro, A. A. Bettelheim, and F. A. Bettelheim, "Water gradients across bovine cornea," *Investigative Ophthalmol. Vis. Sci.*, vol. 29, no. 6, 1988.

[44] R. Turss, J. Friend, M. Reim, and C. H. Dohlman, "Glucose concentration and hydration of the corneal stroma," *Ophthalmic Res.*, vol. 2, no. 5, pp. 253–260, 1971, doi: 10.1159/000264570.

[45] S. M. Thomasy, V. K. Raghunathan, M. Winkler, C. M. Reilly, A. R. Sadeli, P. Russell, J. V. Jester, and C. J. Murphy, "Elastic modulus and collagen organization of the rabbit cornea: Epithelium to endothelium," *Acta Biomater.*, vol. 10, no. 2, pp. 785–791, Feb. 2014, doi: 10.1016/j.actbio.2013.09.025.

[46] J. A. Last, P. Russell, P. F. Nealey, and C. J. Murphy, "The applications of atomic force microscopy to vision science," *Investigative Opthalmol. Vis. Sci.*, vol. 51, no. 12, p. 6083, Dec. 2010, doi: 10.1167/iovs.10-5470.

JOHANNES WENZEL was born in Neustadt am Rübenberge, Hannover, Germany, in 1991. He received the B.Sc. and M.Sc. degrees in physics from Leibniz University Hannover, in 2019, where he is currently pursuing the Ph.D. degree in physics with the Institute of Quantum Optics in Hannover.

From 2014 to 2017, he was a Student Research Assistant at Rowiak GmbH. His research interests include the interaction of tissue with laser light and measurement techniques for rheological properties.

NIKLAS RÜPRICH was born in Hannover, Germany, in 1998. He received the B.Sc. degree in physics from Leibniz University Hannover, in 2021, where he is currently pursuing the M.Sc. degree in light field microscopy.

Since 2021, he has been working as a Student Research Assistant at the Institute of Quantum Optics.

KARSTEN SPERLICH studied physics at the University of Rostock, Rostock, Germany, and received the Ph.D. degree in physics from the University of Rostock, in 2017.

He was a Visiting Researcher at the Liquid Crystal Institute, Kent, OH, USA, in 2006. He currently works with the Department of Ophthalmology, Rostock University Medical Center, Rostock. His research interests include biomedical and biomechanical imaging, ultra-fast laser pulses, laser-tissue interaction, and their relation to ophthalmology.

Dr. Sperlich is a member of the Deutsche Physikalische Gesellschaft, the Deutsche Ophthalmologische Gesellschaft, and the Association for Research in Vision and Ophthalmology.

OLIVER STACHS received the Ph.D. degree in physics from the University of Rostock, Rostock, Germany, in 1996.

Then, follow by a Leopoldina Fellowship for a visiting of the Stanford Synchrotron Radiation Laboratory, Stanford University, USA. In 2012, he was appointed as an Associate Professorship for Experimental Ophthalmology at the University of Rostock. He is currently a Scientific Group Leader of the experimental ophthalmology with the Department of Ophthalmology, University Medical Center, University of Rostock. His research interests include biomedical optics, ultra-high-field MRI, and the development of ophthalmic implants.

MELANIE SCHÜNEMANN was born in Parchim, Germany, in 1988. She received the B.Sc., M.Sc., and Ph.D. degrees in physics from the University of Rostock, Rostock, Germany, in 2010, 2012, and 2018, respectively.

During her Ph.D. studies, she was a Visiting Researcher at the Department of Quantum Science, Australian National University, Canberra, Australia, and the JILA, University of Colorado, Boulder, USA. She is currently working with the Department of Ophthalmology, Rostock University Medical Center, Rostock, where she works on the application of quantum technologies in Brillouin spectroscopy. Her research interests include quantum optics and technologies and their application in life sciences.

Dr. Schünemann is a member of the Deutsche Physikalische Gesellschaft.

COLETTE LEYH was born in Riesa, Saxony, Germany, in 1968.

She has the profession of a Day Care Educator and subsequently worked as a Medical Assistant in an ophthalmology practice, from 1996 to 2007. She moved to the Rostock University Medical Center, Rostock, Germany, in 2007, as a Technical Assistant, and is in charge of the cell culture laboratory.

STEFAN KALIES studied physics at Leibniz University Hannover, Hannover, Germany, and received the Ph.D. degree from the Regenerative Sciences Program, Hannover Medical School, Hannover, in 2016.

Currently, he is a Postdoctoral Researcher at the Institute of Quantum Optics, Leibniz University Hannover, and a Group Leader at the Lower Saxony Centre for Biomedical Engineering, Implant Research and Development. His main research interests include the study of cell repair and tissue regeneration using imaging techniques and laser-based manipulation.

ALEXANDER HEISTERKAMP received the Ph.D. degree in physics.

He is an expert in biomedical optics, with a special interest in nonlinear imaging and manipulation of cells and tissues, laser therapy and diagnostics, and nanoparticle-laser interaction. He holds a professorship for biophotonics at Leibniz University Hannover, Hannover, Germany. Formerly, he was a Professor of physics at Friedrich-Schiller-University in Jena, worked as the Department Head at the Laser Zentrum Hannover, Hannover, and was a Postdoctoral Researcher at the Eric Mazur's Group, Harvard University, USA.

Prof. Heisterkamp is a member of various societies and a fellow of SPIE.